

AtTrm5a catalyses 1-methylguanosine and 1-methylinosine formation on tRNAs and is important for vegetative and reproductive growth in *Arabidopsis thaliana*

Xiaohuan Jin^{1,2}, Zhengyi Lv^{1,2}, Junbao Gao^{1,2}, Rui Zhang^{1,2}, Ting Zheng^{3,4}, Ping Yin^{3,4}, Dongqin Li⁴, Liangcai Peng^{1,2}, Xintao Cao⁵, Yan Qin⁵, Staffan Persson^{6,7}, Bo Zheng⁸ and Peng Chen^{1,2,*}

¹College of Plant Science and Technology, HuaZhong Agricultural University, Wuhan 430070, China, ²Biomass and Bioenergy Research Centre, HuaZhong Agricultural University, Wuhan 430070, China, ³College of Life Science, HuaZhong Agricultural University, Wuhan 430070, China, ⁴National Key Laboratory of Crop Genetic Improvement, HuaZhong Agricultural University, Wuhan 430070, China, ⁵Institute of Biophysics, Chinese Academy of Sciences, China, ⁶School of Biosciences, University of Melbourne, Parkville 3010, VIC, Australia, ⁷Joint International Research Laboratory of Metabolic & Developmental Sciences, Shanghai Jiao Tong University-University of Adelaide Joint Centre for Agriculture and Health, State Key Laboratory of Hybrid Rice, School of Life Sciences and Biotechnology, Shanghai Jiao Tong University, Shanghai 200240, China and ⁸College of Horticulture and Forestry Sciences, HuaZhong Agricultural University, Wuhan 430070, China

Received September 26, 2018; Revised November 15, 2018; Editorial Decision November 17, 2018; Accepted November 20, 2018

ABSTRACT

Modified nucleosides on tRNA are critical for decoding processes and protein translation. tRNAs can be modified through 1-methylguanosine (m¹G) on position 37; a function mediated by Trm5 homologs. We show that *AtTRM5a* (At3g56120) is a Trm5 ortholog in *Arabidopsis thaliana*. AtTrm5a is localized to the nucleus and its function for m¹G and m¹I methylation was confirmed by mutant analysis, yeast complementation, m¹G nucleoside level on single tRNA, and tRNA *in vitro* methylation. *Arabidopsis attrm5a* mutants were dwarfed and had short filaments, which led to reduced seed setting. Proteomics data indicated differences in the abundance of proteins involved in photosynthesis, ribosome biogenesis, oxidative phosphorylation and calcium signalling. Levels of phytohormone auxin and jasmonate were reduced in *attrm5a* mutant, as well as expression levels of genes involved in flowering, shoot apex cell fate determination, and hormone synthesis and signalling. Taken together, loss-of-function of AtTrm5a impaired m¹G and m¹I methylation and led to aberrant protein translation, disturbed hormone homeostasis and developmental defects in *Arabidopsis* plants.

INTRODUCTION

Transfer RNA (tRNA) molecules from all organisms contain modified nucleosides, which are important for correct decoding processes based on codon-anticodon interaction. Modified nucleosides, particularly those around the anticodon loop region, are especially critical for the efficiency and accuracy of translation (1,2). Therefore, knock-out or knock-down mutants of modification enzymes for these nucleosides affect cell growth, temperature sensitivity, metabolism, embryonic development and immune responses in plants (3–5).

1-Methylguanosine (m¹G, methylation of guanosine at the N1 atom) at position 37 of tRNAs is one of the most ancient tRNA modifications (6), and is present also on tRNAs in mitochondria and chloroplasts. In *Escherichia coli* and *Salmonella typhimurium*, TrmD proteins are responsible for the m¹G37 modification (6,7), whereas the same modification is mediated by Trm5 proteins in animals, yeast and archaea (8–10). The importance of m¹G37 is highlighted by its direct function in the decoding process, and deficiency of m¹G at this position causes increased frameshifting errors in several organisms (1,8). Indeed, the requirement of reading frame maintenance might explain the conservation of m¹G37 in tRNAs in many organisms.

The yeast *TRM5* gene was initially identified via an ORF name *YHR070W*, which complemented the temperature sensitive phenotype of the *Salmonella trm5* mutant (8).

*To whom correspondence should be addressed. Tel: +86 27 87281765; Email: chenpeng@mail.hzau.edu.cn

Deletion of the *TRM5* gene in *Saccharomyces cerevisiae* not only severely impaired growth, but also rendered an unmodified G at position 37 of tRNA-Asp-GUC (anticodon GUC), tRNA-Leu-UAG, tRNA-His-GUG and tRNA-Arg-CCG (8). Trm5 proteins belong to Class-I methyltransferases (MTases) with a typical Rossmann fold, and function as monomers (11–13). There are three groups of archaeal Trm5: Trm5a, Trm5b, and Trm5c, of which Trm5b appears to be the likely ancestor of the eukaryotic Trm5 proteins (14,15). The yeast Trm5 protein contains 499 amino acids with 33% similarity to the archaea Trm5 protein (8). X-ray structure of MjTrm5 (Trm5 from *Methanococcus jannaschii*) complexed with the substrate tRNA revealed an AdoMet-binding pocket between the D2 and D3 domains. The E185, R186, D223 and D251 residues of MjTrm5 are highly conserved and critical for guanosine methylation (9,15).

According to the tRNADB (<http://trna.bioinf.uni-leipzig.de/>) (18,19) and the Modomics database (<http://modomics.genesilico.pl/>) (18–20), m¹G is found on at least two different locations in eukaryotic tRNAs: one at position 37 catalysed by a Trm5 enzyme, and the other at position 9 catalysed by a Trm10 protein (21,22). Unlike the TrmD protein, which can only methylate G to m¹G, Trm5 protein can also methylate inosine (I) at position 37 (22). Indeed, the yeast *trm5* mutant lacks m¹I, suggesting that Trm5p catalyses also the transfer of methyl groups to I37 (8). Although the presence of m¹G37 could prevent +1 frameshifting, the absence of m¹G in the yeast *trm5* mutant had no influence on –1 frameshifting (23). While archaea and human Trm5 proteins are located in the cytoplasm, those from *S. cerevisiae* and *Trypanosoma brucei* are located in the mitochondria (24). Reduction of m¹G37 by RNAi in *T. brucei* results in a decrease in mitochondrial protein synthesis (24). m¹G37 modification on mitochondria initiator tRNA-Met is important to prevent translational frameshifting in yeast (25), and similarly in tRNA-Pro-UGG which is naturally prone to +1 frameshift (26).

While we have relatively good knowledge of how tRNA modification affects yeast and prokaryotes, no Trm5 enzyme has been described in the plant kingdom. In this work, we used *A. thaliana* to study the function of m¹G37 methyltransferase(s) and the impact of m¹G37 modification on plant growth and development. Our *in vivo* and *in vitro* data show that AtTrm5a is a tRNA m¹G methyltransferase, and that its function is critical for juvenile growth and floral development in *Arabidopsis*.

MATERIALS AND METHODS

Source material and growth conditions

Arabidopsis Columbia-0 ecotype was used in this study. Salk line seeds (Salk_022617, Salk_012573) were purchased from NASC (the European Arabidopsis Stock Center, now available from ABRIC, <https://abrc.osu.edu/>). Sterilized seeds were sown on $\frac{1}{2}$ MS medium and grown in a culture room, later in soil in growth chamber at 22°C, with 16 h light/8 h dark photo period, with humidity level of 60% and light intensity of 100 $\mu\text{mol m}^{-2} \text{s}^{-1}$.

GBY15 (*Mata, his3D1, leu2D1, met15D0, ura3D0, trm5:KanMX*) and GBY16 (*Mata, his3D1, leu2D1, met15D0, ura3D0, TRM5*) yeast strains were kindly provided by Prof. Glenn Bjork, Umea University. YPD plate was used for yeast plating and growth observation at 30°C.

Bioinformatics analysis of Trm5 homologs

Trm5p from *S. cerevisiae* were used as query sequence to retrieve protein homologs on NCBI database (<https://www.ncbi.nlm.nih.gov/>) by blastp with cut-off value set as 1.0E-6. Multiple sequence alignment was performed by ClustalX 2.0 (<https://www.ebi.ac.uk/Tools/msa/clustalw2/>) and Genedoc software (<http://www.softpedia.com/get/Science-CAD/GeneDoc.shtml>). Non-rooted Neighbourhood Joining tree was constructed with MEGA5.0 software (27), bootstrap analysis was performed with 1000 iterations. Protein secondary structure was predicted by Phyre2 (<http://www.sbg.bio.ic.ac.uk/phyre2/html/page.cgi?id=index>) (28).

Total tRNA isolation and nucleoside analysis

tRNAs were extracted from rosette leaves (100mg fresh weight) of four-week-old seedlings using E.Z.N.A.[™] miRNA Extraction Kit (Omega Bio-Tek Inc.). About 20 μg tRNA was digested with 0.6 U P1 nuclease from *Penicillium citrinum* (N8630, Sigma-Aldrich) and 3 U calf intestine alkaline phosphatase (CAP-101, Toyobo, Japan) in 20 mM HEPES–KOH (pH 7.0) at 37°C for 3 h (29). The resulting nucleoside mix was diluted with MilliQ water to a concentration of 10ng/ μL and 10 μL samples was injected into the LC-MS/MS machine (Shimadzu-Nexera X2). All RNA samples were analysed using three biological replicates, and at least two technical replicates. API 4000 Q-Trap mass spectrometer (Applied Biosystems) coupled with LC-20A HPLC system (Shimadzu) was used for nucleoside separation and detection, and 2 mM ammonium acetate (solution A) and methanol (solution B) as binary solvent system (29). The elution gradient was set up as follows: 0–10 min, 0–50% of B; 10–13 min, 50–100% of B; 13–23 min, 100% of B; 23–23.1 min, 100–5% of B, 23.1–30 min, 5–0% of B. 100% Solution A was applied for 10 min to re-equilibrate the column before the next sample was injected. A DAD detector (190–400 nm) monitored the LC signals from the main nucleosides, whereas ion counts were recorded in positive ion mode in the range of 190–400 (30–32). The retention time (min) for canonical nucleosides, the mass of Q1 and Q3 ions for each modified nucleoside monitored, as well as instrumental parameters (de-clustering potential, collision energy and collision exit potential) were reported previously (32). The abundance of each modified nucleoside was represented by its unique ion peak area, normalized to the sum of the four canonical nucleosides (C, U, G and A nucleosides). Noise level was set as 1.0E+03, i.e. any ion peak under this noise level was not quantified. Since m¹G, m²G and m⁷G have the same Q1 and Q3 mass, they were discriminated by retention time, in the order of m⁷G, m¹G and m²G, respectively. The identity of m⁷G peak was confirmed with external standard (Santa Cruz Biotechnology, Inc. USA),

whereas the identity of m¹G versus m²G was indirectly confirmed with results from yeast *trm5* mutant (8).

AtTrm5a protein purification and tRNA *in vitro* methylation

AtTRM5a full length cDNA was amplified and cloned into pGEX-6P-3 (GE healthcare Life Sciences, Shanghai, China) using Sall and NotI restriction sites (Supplementary Table S1), resulting in GST-AtTrm5a fusion protein. Expression of the fusion protein was performed in *E. coli* strain BL21 with 0.5 mM isopropyl β-D-1-thiogalactopyranoside (IPTG) and subsequently purified with ProteinIso GST Resin (Transgen Biotech, Beijing, China). Substrate tRNAs were *in vitro* transcribed with T7 polymerase (Riboprobe[®] *in vitro* transcription systems, Promega). *In vitro* methylation was performed in the presence of 100 mM Tris-HCl, 5 mM MgCl₂, 100 mM KCl, 4 mM DTT, 0.1 mM EDTA, 0.024 mg/ml BSA and 25 μM AdoMet. Substrate tRNAs were provided in 10 μM, and AtTrm5a protein in 1 or 2 μM (22,25). *In vitro* methylation was performed at 37°C for 1 h, with three technical repeats.

Genetic complementation and protein subcellular localization

AtTRM5a cDNA was amplified and cloned into pD1301s using KpnI and Sall sites and in frame with downstream eGFP gene (Supplementary Table S1). *AtTRM5a-GFP* fusion gene driven by 35S promoter was used for genetic complementation of *atrm5a* mutant, since rather low expression was observed with endogenous promoter. Hyg positive seedlings were isolated from T1 generation. T2 progeny was used for gene expression by qRT-PCR, m¹G and m¹I nucleoside abundance were determined by LC-MS as described above.

The *AtTRM5a-GFP* construct was used for AtTrm5a subcellular localization using T1 transgenic seedlings. Four-day-old seedlings grown on MS plate were used for imaging, roots were excised and mounted with water, and root epidermis cells were examined by Leica TCS SP8 confocal microscope. The AtTRM5a-GFP, AtTRM5a-D1-GFP and AtTRM5a-D1D2-GFP constructs were used to transform *Agrobacterium* GV3101. The *Agrobacterium* strains harboring either of the three constructs were used to infiltrate lower epidermal cells of four-week-old *Nicotiana benthamiana* leaves (33). Leaves were examined 48–72 h after infiltration using OLYMPUS IX71 fluorescence microscope. 4',6-Diamidino-2-phenylindole (DAPI) staining was used as a nuclear marker. We applied DAPI staining on seedlings for 20 min at room temperature. The excitation and emission wavelengths for DAPI were 385 and 420 nm, respectively; and for GFP, 470–490nm and 500–540 nm, respectively.

Hormone extraction

Samples (three biological replicates) were taken from 4-week- or 7-week-old seedlings. Hormone extraction and quantification was conducted according to Liu *et al.* with minor modifications (34). Extracted hormones from wild type or *atrm5a* mutant was dried by evaporation under nitrogen flow for 4 hrs at room temperature, dissolved in 200 μL methanol and quantified using LC-MS. Hormones were

separated on an Shim-pack VP-ODS column (2.1 mm × 150 mm, 5 μm particle size; Shimadzu) using API 4000 Q-Trap mass spectrometer coupled with LC-20A system (Shimadzu). The injection volume was 10 μL. The binary solvent system consisted 0.1% acetic acid in H₂O (solvent A) and 0.1% acetic acid in MeCN (solvent B), with a constant flow rate of 0.25 mL/min. The elution gradient was set up as the following: 0–10 min, 5–100% B; 10–15 min, 100% of B; 15–15.01 min, 100–5% of B; 15.01–20 min, 5% B. Hormones were scanned in negative ion mode.

Real-time PCR

For verifying gene expression, four-week-old seedlings from wild type or *atrm5a* mutant were sampled with three biological replicates. Samples were flash-frozen and ground into powder in liquid nitrogen. Around 100 mg powder (fresh weight) was used for total RNA extraction using the RNAPrep pure Plant Kit (Tiangen Biotech, Beijing, China). DNase I treatment was included in RNA extraction procedure. RNA yield and purity was assessed by NanoPhotometer-N60 (Implen Inc, Germany). cDNA synthesis was performed by oligo(dT)18 priming with M-MLV RTase (TaKaRa, Dalian, China). Sequence and amplicon length of RT-qPCR primer were listed in Supplementary Table S1. RT-qPCR was performed using 2× Sybr-green Master Mix (Life Technology) in a Bio-Rad IQ5 real-time PCR system (Life Science, Wuhan, China). For all primer pairs, an annealing temperature of 59°C was set in a three step protocol (95°C 15 s; 59°C 15 s; 72°C 30 s). Relative changes of RNA abundance were determined by the ΔΔCt method using At1g13440 (*AtGAPC2*) and At5g60390 (*AtEF1a*) for normalization (35). Relative expression was calculated from three biological replicates and two technical replicates.

Yeast complementation

The cDNA fragments of *AtTRM5a* was amplified and cloned into pYPG15 vector using KpnI and Sall sites. The resulting plasmid was transformed into *Δtrm5* mutant strain GBY15 (*Mata*, *his3D1*, *leu2D1*, *met15D0*, *ura3D0*, *trm5*: *KanMX*) and congenic wild-type GBY16 (*Mata*, *his3D1*, *leu2D1*, *met15D0*, *ura3D0*, *TRM5*) using URA3 as selection marker. The resulting strain (GBY15+*AtTRM5a*) was analysed for growth phenotype and m¹G nucleoside by LC-MS. with three biological replicates.

Ribosome profiling

Polysomes were extracted from 4-week-old seedlings with minor modifications (36). Rosette leaves from wild type and *atrm5a* mutant were sampled with three biological replicates and flash frozen in liquid nitrogen. For each polysome extraction, 350–500 mg samples were manually ground with 1 ml polysome isolation buffer containing 200 mM Tris-HCl, pH 8.4, 50 mM KCl, 25 mM MgCl₂, 1% deoxycholic acid, 2% polyoxyethylene 10 tridecyl ether, 300 μg/ml Heparin, 1% Triton X-100, 1% Tween-20, 50 μg/ml μg/ml cycloheximide (stock solution dissolve in DMSO). A 15–45% sucrose gradient was prepared using BIOCAMP Gradient

Master ip-107. After first spin in SW40 Ti rotor at 20 000g at 4°C for 15 min in Beckman Coulter centrifuge, 12.0–14.0 OD₂₆₀ samples were loaded on a second 15–45% sucrose gradient and spun in SW40 rotor at 36 000 rpm (163 659g) at 4°C for 5 h in a BECKMAN Optima L-80 XP Ultracentrifuge. *A*₂₅₄ absorbance from the resulting fractions were monitored by an in-house gradient fractionator with BIO-RAD ECONO PUMP EP-1 coupled with Shanghai HuXi HD-4 UV detector and chart recorder. RNA was extracted from polysome fractions and subsequently used in real-time PCR analysis.

Proteomic analysis using iTRAQ method

Four-week-old seedlings of wild type and *atrm5a* mutant were used for total protein extraction. Three biological replicates were taken, 100 µg protein was used for each replicate. Proteins were labelled with iTRAQ tags 113–118 during trypsin digestion (37). Labelled peptides were fractionated by reverse-phase liquid chromatography followed by orbitrap Q Exactive MS/MS (Thermo Scientific). Proteome Discoverer 1.4 software was used for data analysis. Peptide sequence alignment was performed against TAIR10_pep_20101214.fasta database. Mascot (Matrix Science, version 2.3.2) was searched with fragment ion mass tolerance of 0.1 Da and peptide mass tolerance of 20.0 ppm. Proteins with fold change ≥ 1.20 or ≤ 0.80 and significance level $P \leq 0.05$ were considered to be differentially expressed. DEP proteins were annotated against GO and KEGG database (www.genome.jp/kegg/) for function annotation; category enrichment was performed using Blast2GO (38), with FDR value 0.05 by Fisher's Exact Test, or P value 0.05 by student's t -test.

Structure modelling of AtTrm5a

Using sequence conservation in the Trm5p homologs, a structure model of AtTrm5a was created by alignment with PDB 2YX1_A (Chain A of a Trm5 from *Methanococcus jannaschii*). Critical amino acids around the catalytic centre are shown with stick model, with different atoms color-coded. Numbering of amino acid corresponds to their position in AtTrm5a coding sequence. AdoMet binding pocket is located between E206, R209, N380, P382, Y198 and R165. Due to the flexibility of D1 domain, model is projected using only D2 and D3 domains. Figure prepared using program PyMOL (The PyMOL Molecular Graphics System, Version 2.0 Schrödinger, LLC., <https://pymol.org/2/>).

RESULTS

Identification of a Trm5 homolog in Arabidopsis

m¹G37 nucleoside modification is catalysed by Trm5p in *S. cerevisiae* (10). Based on protein sequence homology, two candidate genes were identified in *A. thaliana*, with blastp value above 1.0E–06 (39). At3g56120 was the best candidate, with 2E–59 E -value and 49% similarity on protein sequence level to Trm5p. At3g56120 was therefore tentatively named AtTrm5a, while the second-best hit (At4g27340) was named AtTrm5b (Figure 1A). Protein domain analysis suggested that AtTrm5a has three structural domains; D1, D2

and D3 domains (D3 referred to as MTase domain) (Figure 1B). Several amino acid residues within the D3/MTase domain are critical for binding to AdoMet or for recognition of guanosine 37 on substrate tRNA, such as R145, D172, E185 and D223 in MjTrm5 protein (Figure 1C) (16,17). These residues are conserved in the plant Trm5p homologs (red asterisk, Figure 1B).

To investigate if AtTrm5a is involved in tRNA methylation we ordered T-DNA mutants that were indicated as affecting the gene from NASC (<http://arabidopsis.info/>). Salk_022617 carries a T-DNA insertion in the eighth exon of *AtTRM5a* (Supplementary Figure S1), and homozygous progeny for the insert has substantially reduced *AtTRM5a* transcripts (Figure 1D). We isolated and digested tRNA from the mutant and wild-type, and analysed it for modified nucleosides. In the *atrm5a* mutant, the m¹G nucleoside level was reduced to 42% of that in wild type (Figure 1E). Notably, the level of m¹I nucleoside in the *atrm5a* mutant was reduced to 9% of that in wild type (Figure 1E), suggesting that AtTrm5a is also involved in I to m¹I methylation, similar to what has been found in *S. cerevisiae* (10). Complementation of the T-DNA line using an *AtTRM5a* cDNA rescued the level of these two methylated nucleosides, confirming that the biochemical phenotype is due to the loss of *AtTRM5a* (Figure 1E). We also attempted to analyse mutants for AtTRM5b; however, we were not able to isolate *atrm5b* knock-out mutant from Salk_012753 due to lethality in homozygous state (Supplementary Figure S2).

mRNA and rRNA also contains methylated nucleoside, especially m¹A, m⁶A and m⁵C modifications (40–42). Particularly, methylated nucleosides on mRNAs function as epitranscriptomic markers and play important roles for gene expression regulation (43,44). To corroborate the function of AtTrm5a on tRNA substrate instead of rRNA or mRNA, total RNAs were fractionated from WT and *atrm5a* mutant, separated into sRNAs and other RNAs, collected separately and analysed for m¹G and m¹I modifications (Supplementary Figure S3). We found that the majority of m¹G and m¹I were associated with sRNA, and not mRNA or rRNA, suggesting that AtTrm5a methylation activity mainly affects tRNAs.

AtTrm5a can methylate yeast tRNA *in vivo* and *in vitro*

To confirm the activity of AtTrm5a as a m¹G methyltransferase, we attempted to complement a yeast $\Delta trm5$ mutant with the *AtTRM5a* gene. Yeast GBY15 mutant is defective for m¹G37 nucleoside modification, and the mutant strain grows slow compared to the congenic strain GBY16 (8). We cloned the full-length coding region of *AtTRM5a* into the yeast expression vector pYPGE15, and subsequently transformed it into GBY15 (Figure 2A). We found that the mutant growth was rescued by the *AtTRM5a* (Figure 2B). Notably, the *AtTRM5a* could also rescue the m¹G nucleoside level in the GBY15 (Figure 2C).

Yeast Trm5p can methylate tRNA-Asp-GUC, tRNA-Leu-UAA, tRNA-Leu-UAG, tRNA-His-GUG and several other tRNA isoacceptors (8). Because no Arabidopsis tRNA has been sequenced, we first used yeast tRNA-Asp-GUC as substrate for *in vitro* methylation (Figure 2D). AtTrm5a was expressed as a GST fusion protein in *E. coli*

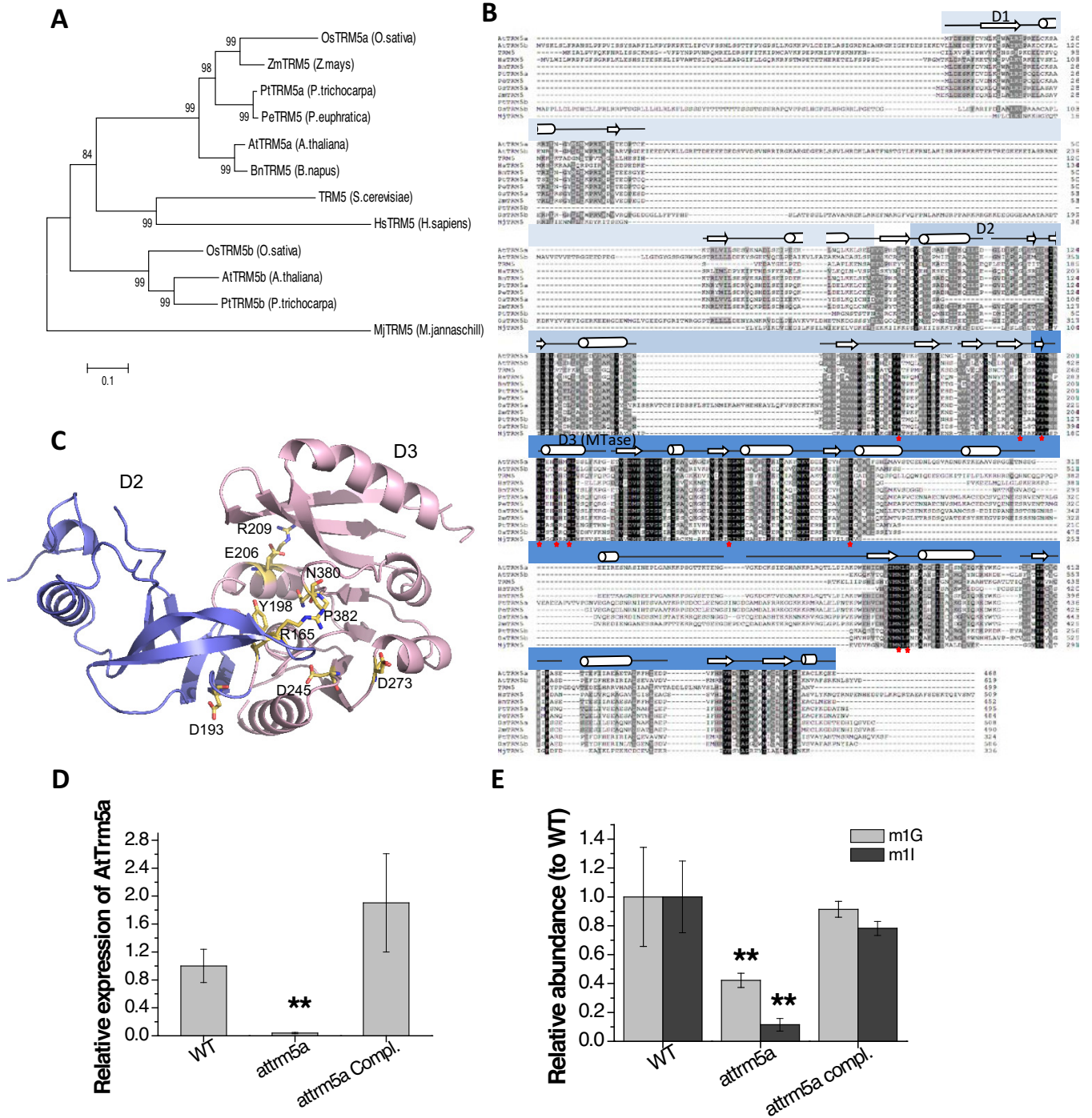


Figure 1. Identification of Trm5 homologs and characterization of *attrm5a* mutant. (A) Unrooted neighbour-joining tree of plant Trm5 homologs. Bootstrap analysis performed with 1000 iterations, supporting values were indicated at each branching point. (B) Multi-sequence alignment of plant Trm5 homologs. Protein secondary structure predictions are illustrated above, with D1, D2 and D3 (MTase) domains shown in different colours. Amino acids critical for AdoMet or tRNA binding are highlighted with red asterisks. (C) Prediction of AtTrm5 protein structure. Only D2 (in blue ribbons) and D3 (in pink ribbons) domains were shown, D1 domain is highly flexible therefore not included. Critical amino acids were shown in stick model. (D) *AtTRM5a* relative expression in *attrm5a* mutant and complemented plants. Three biological replicates and two technical repeats are included. (E) Quantification of m¹G and m¹I nucleoside in *attrm5a* mutant and complementing plants. ** indicated significant difference at $P \leq 0.01$ by Student's *t*-test.

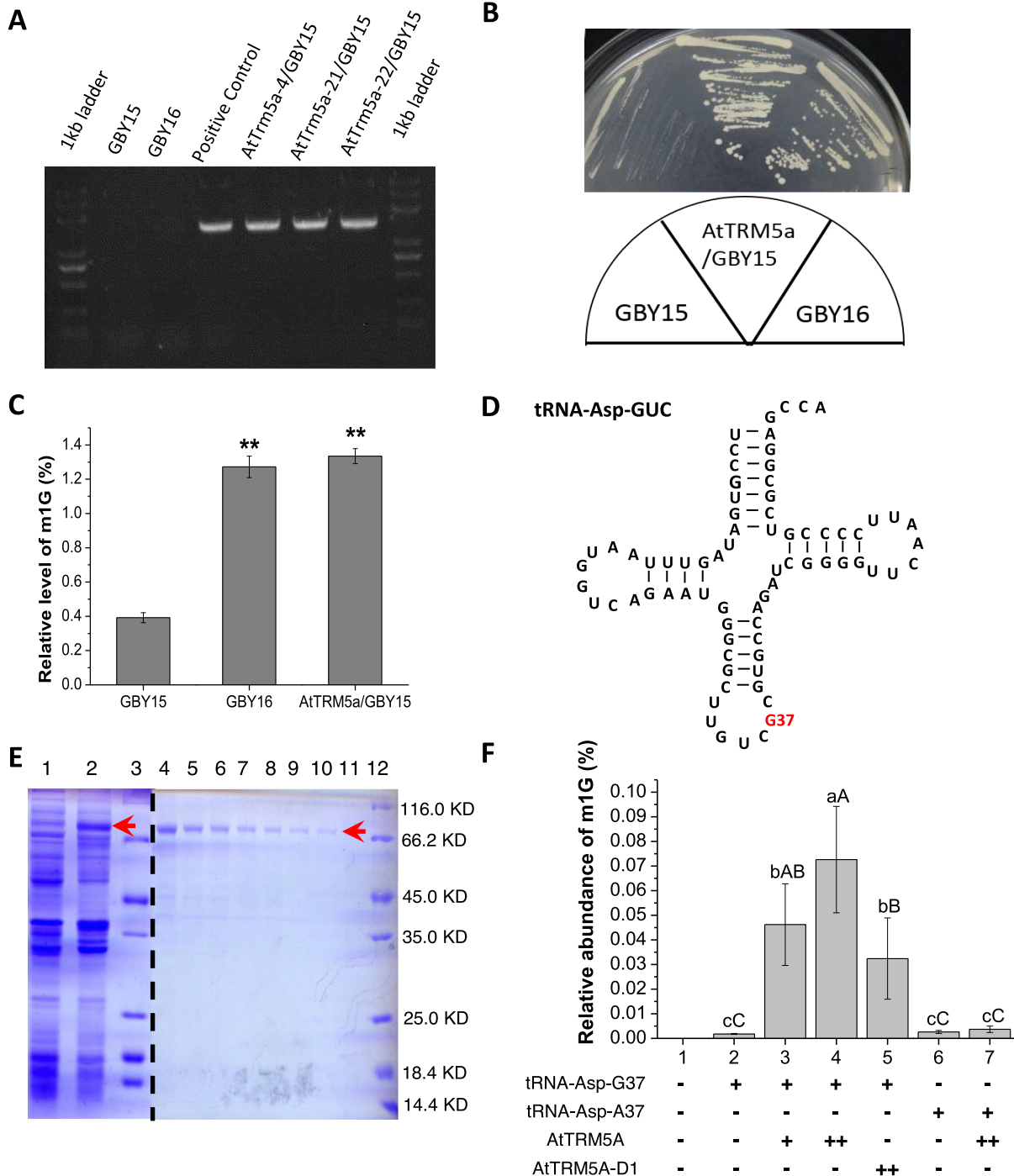


Figure 2. *In vivo* and *in vitro* analysis of AtTrm5a for tRNA methylation activity. (A) PCR verification of yeast strains complemented by *AtTRM5a*. GBY15, $\Delta trm5$ mutant; GBY16, congenic wild type. AtTRM5a-4, AtTRM5a-21, AtTRM5a-22 were three independent complemented strains. Positive control, *AtTRM5a* plasmid construct. (B) Growth of yeast strains on YPD plate at 30°C for three days. Panel below indicated strains in each plate sector. (C) Quantification of m¹G nucleoside level by LC-MS. Three individual clones are used, three technical repeats were included. ** indicates significant difference at $P \leq 0.01$ by Student's *t*-test. (D) Substrate tRNA used for *in vitro* methylation (yeast tRNA-Asp-GUC). Guanosine at position 37 is highlighted. (E) SDS-PAGE gel for expression and purification of AtTrm5a-GST. Protein size markers are shown on the right. The expected size of AtTrm5a-GST is indicated with arrows. Lane 1: total protein from cell extract; Lane 2: total protein after IPTG induction; Lane 3 and 12, protein size marker; Lane 4–11, eluted GST-AtTrm5a. Dotted lines indicate separate gels. (F) Quantification of m¹G nucleoside with different substrate and protein. Y axis indicates percentage of m¹G peak area to the sum of U, C, G and A nucleosides. tRNA-Asp-A37 is a mutated tRNA-Asp with adenosine at position 37. AtTRM5a-D1, truncated AtTrm5a protein with deletion of D1 domain. + or ++ indicated relative abundance of tRNA substrate or AtTrm5a proteins. Multiple comparison was used, small or capital letters indicate significant difference at $P \leq 0.05$ or $P \leq 0.01$, respectively.

and purified using a Glutathione-labelled column (Figure 2E). The fusion protein was subsequently eluted from the column (ca. 78 kDa, arrows in Figure 2E), and different amounts of the fusion protein was added in *in vitro* methylation assays (Figure 2F). We generated the substrate tRNA-Asp-GUC by *in vitro* transcription by T7 polymerase, using S-adenosyl-methionine (AdoMet) as methyl donor (9,25). Since the protein domain structure of AtTrm5a aligns with previous studies on a/eTrm5 proteins and the MjTrm5b tertiary structure (10,45), we generated two truncated version of AtTrm5a in which we could test the functional importance of D1 and D2 domains in relation to MTase activity. As shown in Figure 2, we detected clear m¹G activity when full-length AtTrm5a protein was provided in a dosage dependent manner (Figure 2F). m¹G was also produced with AtTrm5a-D1, i.e. when only the D1 domain was deleted (Figure 2F), indicating that D1 is not important for MTase activity of the protein. However, due to the unstable condition of the protein when both the D1 and D2 domains were deleted, we were unable to apply it in methylation assays. To test the specificity of methylation on Guanosine at position 37, we also mutated the substrate tRNA-Asp-GUC. When this substrate (tRNA-Asp-A37) was used, no m¹G was detected (Figure 2F), suggesting that the methylation occurs at a Guanosine at position 37.

Although yeast tRNA-Asp-GUC could be methylated by AtTrm5a, the endogenous tRNA-Asp-GUC in Arabidopsis does not contain a G at position 37 (Supplementary Table S2). Based on tRNA sequence from the PlantRNA database, tRNA-His-GUG, tRNA-Leu-CAA and tRNA-Pro-UGG have G37 that might be methylated to m¹G37 by AtTrm5a (Supplementary Table S2). We also noted that mitochondrial and chloroplast tRNA-His-GUG, tRNA-Leu-CAA and tRNA-Pro-UGG have different primary sequence as the nuclear iso-acceptors, indicating that a different set of enzymes might be working in these subcellular compartments. Therefore, we chose tRNA-His-GUG (nuclear encoded), tRNA-Leu-CAA (nuclear encoded) and tRNA-Pro-UGG (mitochondria) for *in vitro* methylation assays, using yeast tRNA-Leu-CAA as control (Figure 3). We found that both tRNA-Leu-CAA (nuclear encoded) and tRNA-His-GUG (nuclear encoded) could be methylated. Notably, the tRNA-His-GUG appears to be a preferred substrate as compared to the yeast tRNA-Asp-GUC, tRNA-Leu-CAA, and Arabidopsis tRNA-Leu-CAA. AtTrm5b (At4g27340) is predicted to be located in mitochondria. However, when we used column-purified GST-AtTrm5b for *in vitro* methylation, no m¹G was produced either with yeast tRNA-Leu, Arabidopsis tRNA-Leu, tRNA-His, or mitochondrial tRNA-Pro-UGG (Figure 3). While we did not detect any MTase activity of AtTrm5b in our assays, we can not rule out that it acts as an MTase *in vivo*.

To verify the function of AtTrm5a on tRNA substrates *in vivo*, we used 5'-biotin-labeled probes complementary to Arabidopsis tRNA-His-GUG or tRNA-Leu-CAA to fish out single tRNA from wild type or *atrrm5a* mutant cells (46). The tRNAs (tRNA-His-GUG or tRNA-Leu-CAA) were subsequently analysed for the abundance of m¹G nucleoside, together with other nucleosides present on the tRNAs (Supplementary Figure S4). In agreement with RNA sequences for tRNA-His-GUG (*Lupinus luteus*, cy-

toplasmic) from the Modomics database, we found that dihydrouridine (D), pseudouridine (Ψ) and 5-methyluridine (m⁵U), m¹G, m¹A and m²A to be associated with tRNA-His-GUG, but the m¹G level was reduced by 95% in the *atrrm5a* mutant compared to wild type (Supplementary Figure S4). As for tRNA-Leu-CAA, we detected m¹G, m¹A, m⁵C, m²G, Um and ac⁴C nucleosides, consistent with cytoplasmic tRNA-Leu-CAA from *Phaseolus vulgaris* from the Modomics database. The m¹G level in tRNA-Leu-CAA was reduced by 75% in the *atrrm5a* mutant compared to wild type (Supplementary Figure S4). Therefore, the m¹G modification on single tRNAs was substantially reduced in the *atrrm5a* mutant, supporting our *in vitro*-based results and biological significance of AtTrm5a in *Arabidopsis*.

AtTrm5a protein is located in the nucleus and is important for plant growth

Previous studies showed that the *T. brucei* Trm5 protein was localized to the nucleus and mitochondria, whereas the yeast Trm5p protein was localized in the cytoplasm and mitochondria (24,25). To clarify the AtTrm5a subcellular localization, a C-terminal GFP tag was fused to its coding sequence (AtTrm5a-GFP) and transformed into the *atrrm5a* mutant plants. This construct rescued the mutant phenotypes (Figure 4K–M), and we therefore monitored the subcellular localization of the protein in root epidermal cells (Figure 4A–H). GFP signal was primarily located within the nucleus and co-localized with DAPI staining (Figure 4D and H).

These data were confirmed using transient infiltration of AtTrm5a-GFP in tobacco leaves (Supplementary Figure S5). To test whether deletion of D1 or D2 caused changes in subcellular distribution of the protein, we created two truncated version of AtTrm5a, removing the D1 or D1+D2 domain(s) from the N-terminal (Figure 1C). Deletion of only D1 did not influence the nuclear localization of the protein as per transient tobacco leaf infiltration, corroborating that the truncated protein is functional (Figure 2F) and is in the correct cellular location. However, similar to above, deletion of both D1 and D2 did not result in any observable fluorescent signal, neither in the nucleus nor in the cytoplasm (Supplementary Figure S6), possibly due to decreased protein stability.

The *AtTRM5a* gene is highly expressed in fast-growing tissues, including shoot apex and root tips (Supplementary Figure S7), which is consistent with expression profiles from the Arabidopsis eFP browser (http://bar.utoronto.ca/efp_arabidopsis/cgi-bin/efpWeb.cgi). *atrrm5a* knock-out mutant showed reduced vegetative growth at the juvenile growth stage (Figure 4I). Fresh-weight of four-week-old seedlings was reduced by 60% in the *atrrm5a* mutant as compared to wild-type (Table 1), and the rosette leaf blade width and length were reduced by 44% and 25%, respectively. Hence, the length/width ratio of leaf blade was reduced in the *atrrm5a* mutant (Table 1). Growth of roots and hypocotyls was also reduced in the mutant (Figure 4J, Table 1). We did not find any significant difference in size of epidermis and palisade leaf cells compared to wild-type, and we therefore attribute the reduction in rosette leaf to a re-

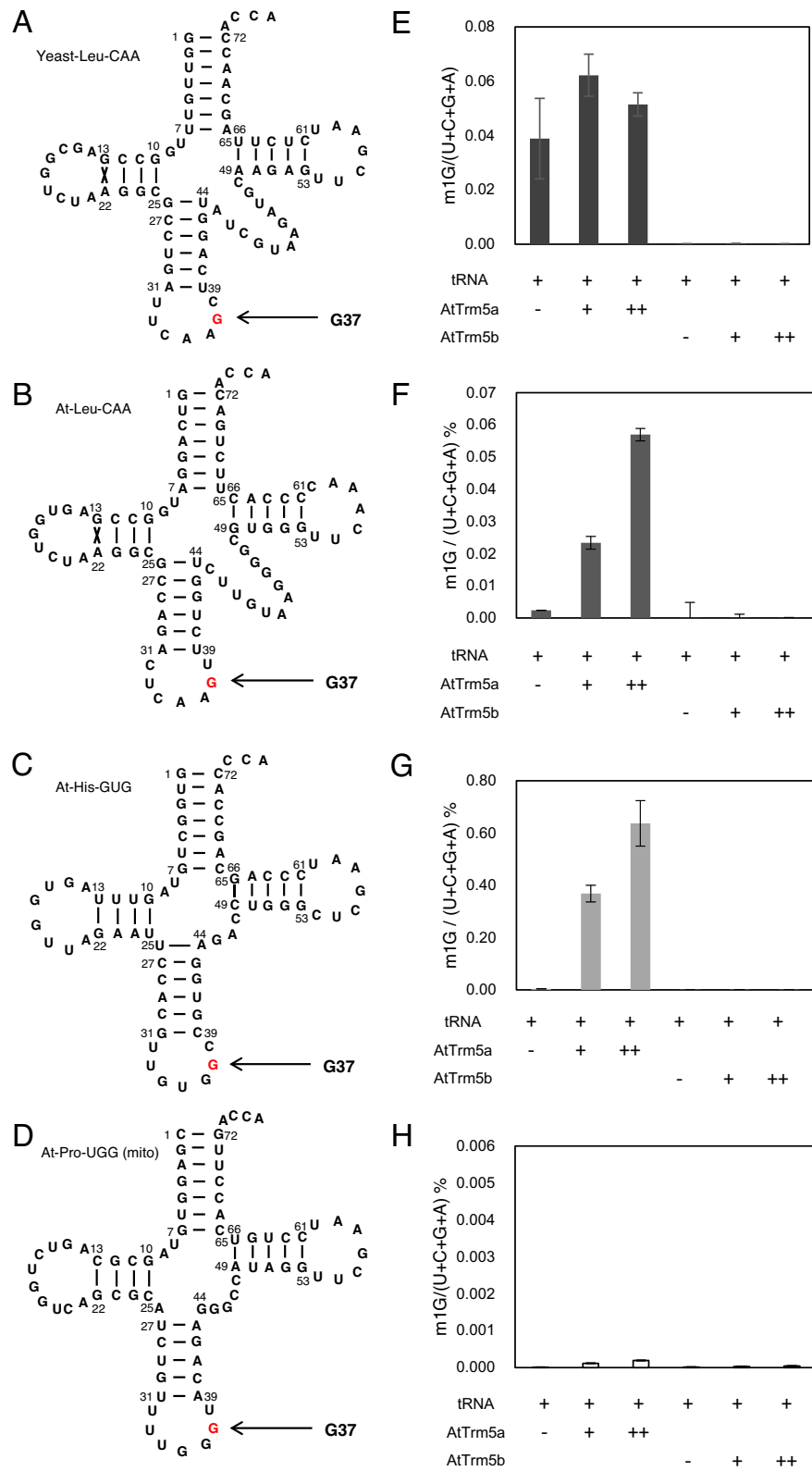


Figure 3. *In vitro* methylation of Arabidopsis tRNA-His, tRNA-Leu and tRNA-Pro (mito) by 5 AtTrm5a and AtTrm5b (A–D) Cloverleaf structure of yeast tRNA-Leu-CAA, Arabidopsis tRNA-Leu-CAA, tRNA-His-GUG and tRNA-Pro-UGG (mito). Guanosine at position 37 (red) are marked with arrows. (E–H) Quantification of m¹G production by LC–MS. + or ++ indicated two different input of proteins. Data retrieved from three independent experiments.

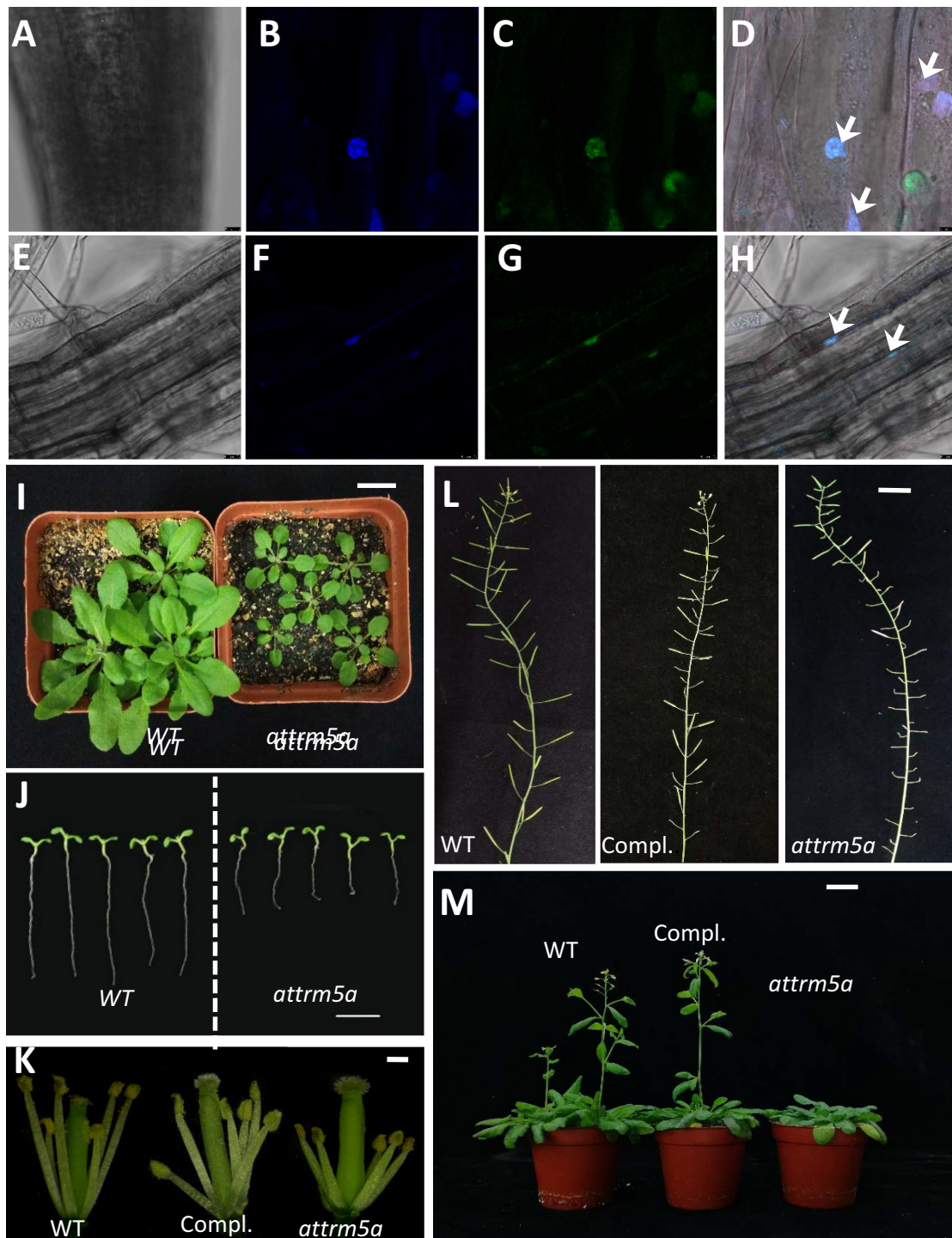


Figure 4. Characterization of AtTrm5a function in plant. (A–H) AtTrm5a protein subcellular localization in root epidermis cells of 4-day-old seedlings. A and E, bright field; B and F, eGFP; C and G, DAPI staining; D and H, merge image of eGFP and DAPI. Arrows indicate co-localization of eGFP with DAPI signals. Scale bar for A–D, 5 μ m; scale bar for E–H, 10 μ m. (I) Dwarf phenotype of 4-week-old *atrm5a* plants. Scale bar 2 cm. (J) Root length on MS plate for 8-day-old seedlings. Scale bar, 1 cm. (K) Short filament phenotype of wild-type, *atrm5a* and complemented plants. Sepal and petals were artificially removed. Scale bar, 200 μ m. (L) Siliques of wild-type, *atrm5a* and complemented plants. Scale bar, 2 cm. (M) Plant height of 7-week-old wild-type, *atrm5a* and complemented plants. Scale bar, 2 cm.

duction in cell division rather than cell expansion (Supplementary Figure S8).

During reproductive growth, *AtTRM5a* expression was also high in flower buds (Supplementary Figure S7). Indeed, stamen filament length in *atrm5a* mutant flowers was shorter compared to wild type (Figure 4K), resulting in poor seed-setting in the young siliques (Figure 4L). However, pollen morphology was not affected in the mutant (Supplementary Figure S9), and we did not detect any differences in transmission efficiency during reciprocal crosses to wild-type plants. The short filament phenotype gradually recovered during later stages, and mature *atrm5a* flowers thus had similar filament length as wild-type, and the siliques then contained similar number of seeds as the wild-type (Figure 4L). Plant height at flowering stage in *atrm5a* mutant was only slightly shorter than wild-type plants (Table 1), but the *atrm5a* mutant bolted much later than wild type (Figure 4M). Notably, the growth phenotypes were restored in the *AtTRM5a* complemented lines (Figure 4K–M).

***atrm5a* mutant has reduced auxin levels**

Hormones are essential for plant growth and development (47–49). In particular, auxin and jasmonate are very important for filament elongation and leaf expansion (50,51). Indole-3-acetic acid (IAA) is the most abundant and physiological relevant form of auxin, it is made in cytosol and chloroplast at shoot apex and young leaves and transported to other tissues by auxin transporters and the vasculature (47). There are many types of IAA conjugates in the cell, among which IAA-Asp (IAA conjugated with Aspartic acid) is an irreversible degradation product (47). On the contrary, Jasmonate (JA) and JA-Ile (JA conjugated with Isoleucine) are made in peroxisome and cytosol, respectively (52). Binding of JA-Ile by its receptor COI1 and JAZ proteins initiates the JA signaling pathway (52). We argued that changes in these hormones might contribute to the dwarf and filament phenotype of the *atrm5a* mutant plants. We therefore collected rosette and flower samples from the *atrm5a* mutant and wild type to compare their levels (Figure 5A to D). We found that IAA levels in four-week-old *atrm5a* mutant plants were significantly lower than in the wild type, concomitantly IAA-Asp levels were significantly higher (Figure 5A and B). JA and JA-ILE levels in four-week-old rosette leaves displayed similar patterns as for IAA and IAA-Asp although not significant, the levels in seven-week-old rosette leaves and flower buds were similar between mutant and wild-type (Figure 5C and D). We also measured the levels of several other hormones, including salicylic acid (SA) and abscisic acid (ABA), but did not detect any significant changes (Supplementary Figure S10).

To see if we could detect any differences in transcripts that could contribute to the impaired filament growth, we took rosette leaves and flower buds from *atrm5a* mutant and wild-type plants, and undertook qPCR of genes involved in floral transition, stamen filament elongation, and shoot apex size control, along with genes involved in JA and IAA synthesis (Figure 5E). Among flowering-related and filament growth controlling genes, *LFY*, *AP3*, *AG* and *BAM1* were significantly reduced in the *atrm5a* mutant compared

to wild-type. *FT* gene expression was also down-regulated in seven-week-old *atrm5a* mutant. Notably, Bam1 protein abundance was also reduced as assessed by proteomics analysis (At5g65700, *atrm5a*/wild-type, 0.783, Supplementary Table S3). Among shoot apex size control genes, only *CUC1* was down-regulated in four-weeks-old *atrm5a* mutant (Figure 5E). *DAD1*, the first gene in JA biosynthetic pathway, was slightly reduced in 4-weeks-old mutant plant. Notably, the key auxin biosynthesis-related gene *YUC1* was reduced significantly in *atrm5a* mutant; however, no differences for *AUX* or *YUC6* were detected in the mutant compared to wild-type (Figure 5E).

Proteins involved in photosynthesis, ribosome biogenesis and calcium signalling are affected in the *atrm5a* mutant

To investigate if global translation was affected, we performed ribosome profiling between WT and *atrm5a* mutant. We used four-week-old seedlings from wild type and *atrm5a* mutant for polysome preparation followed by sucrose gradient separation by ultra-centrifugation. The distribution of 40s, 60s ribosomal subunits, as well as 80s monosomes and polysomes were monitored by UV absorbance (36). Fractions from *atrm5a* background showed more 40s and 60s ribosomal subunits, and more polysomes compared to wild type (Figure 6A). Since translation cannot occur unless 40s and 60s subunits are joined together, the *atrm5a* mutant is likely having a disturbed translation machinery, and might perhaps try to compensate for the loss of tRNA methylation by using more polysomes for protein translation.

To investigate if we could see differences in protein levels due to the defects in m¹G, we used the iTRAQ method for proteomic analyses on four-week-old plants (Figure 6B–E). We recorded a total of 60,284 peptide spectrum matches (PSM), among which 30,468 peptides and 26,926 unique peptides were recorded. Using blastp search against the TAIR_pep database (<https://www.arabidopsis.org/Blast/index.jsp>), we identified 5,699 protein groups. We defined differentially expressed proteins (DEPs) using the following criteria: 1) fold-change ≥ 1.20 or ≤ 0.80 , 2) significance level $P < 0.05$. A total of 293 DEPs were identified (Supplementary Table S3), as shown in a Volcano plot (Figure 6B). Among these DEPs, 102 were more abundant in the *atrm5a* mutant compared to wild-type, whereas 190 proteins were less abundant (Figure 6C). We performed GO annotation of DEPs, and found enriched GO terms associated with chloroplast, thylakoid and photosynthesis (Figure 6D). Meanwhile, KEGG annotation and enrichment analysis revealed three KEGG pathways: ko00195 (photosynthesis), ko04924 (renin secretion) and ko04020 (calcium signaling pathway) (Figure 6E). The proteomics data suggested that proteins with reduced abundance in the *atrm5a* mutant were mainly associated with photosynthesis, ribosome function, and in cell signaling pathways.

A subset of the most affected proteins is shown in Table 2, with protein abundance ratio ≤ 0.60 or ≥ 1.40 between *atrm5a*/wild type (Table 2). The top down-regulated proteins were transcription factors (3 out of 12), cell wall or cell membrane proteins (2 out of 12), and signaling or stress related proteins (3 out of 12). The most affected pro-

Table 1. Growth comparison between wild type and *atrm5a* mutant plants

	WT	<i>atrm5a</i>	<i>atrm5a</i> vs. WT
Fresh weight (g) ^a	0.28 ± 0.03	0.11 ± 0.04**	−60%
Plant height (cm) ^b	39.69 ± 2.70	38.76 ± 1.63	−0.2%
Number of rosette leaves at bolting	15.00 ± 2.00	19.00 ± 2.00**	26%
Leaf blade length (cm) ^c	3.76 ± 0.26	2.1 ± 0.32**	−40%
Leaf blade width (cm) ^c	1.78 ± 0.17	1.33 ± 0.19**	−25%
Leaf blade length/width	2.12 ± 0.14	1.59 ± 0.15**	−25%
Root length (cm) ^d	1.71 ± 0.60	1.00 ± 0.15**	−41%
Hypocotyl length (cm, Dark 8d) ^e	1.53 ± 0.31	1.39 ± 0.28	−9.2%

^aFresh weight of 4 weeks-old seedlings.

^bPlant maximum height at flowering stage.

^cLength and width of the fifth rosette leaf at 4 weeks-old.

^dRoot length measured after 8 days of growth under light conditions.

^eHypocotyl length measured after 8 days of growth under dark conditions.

**Indicate significant difference between mutant and WT by Student's *t* test, $P \leq 0.01$

tein, At5g47380.1, is a protein of unknown function with DUF547 domain. At5g47380.1 is predicted to be located in the nucleus, and the corresponding gene expression profile is very similar to that of *AtTRM5a*, suggesting possible functional connection. To try to find if certain codons were more affected in the *atrm5a* mutant we calculated codon usage frequency using CDS sequence from DEPs. However, we did not find a significant codon bias either in up- or down-regulated proteins (Supplementary Figure S11).

DISCUSSION

In this work, we identified a nuclear-localized m¹G nucleoside MTase (AtTrm5a) that methylate guanosine at position 37 in tRNAs. We show that this enzyme is crucial for Arabidopsis growth, possibly linked to the ability of AtTrm5a to maintain the expression and translation of proteins involved in hormone synthesis, ribosome biogenesis, photosynthesis and cellular signalling pathways. Our data illustrate that the absence of m¹G and m¹I nucleoside on certain tRNA species lead to changes on translation machinery, transcription of genes in shoot apical meristem control, flowering control and hormone synthesis, sequentially manifested by alteration of plant growth and development. Although AtTrm5a is nuclear located, it can, apparently, synthesize m¹G on tRNA-His-GUG, tRNA-Leu-CAA (nuclear genome encoded and transcribed within the nucleus) and most likely also tRNA-Pro-UGG. Given the nuclear localization of AtTrm5a protein, and its *in vitro* methylation activity towards endogenous tRNA-His-GUG and tRNA-Leu-CAA, the m¹G37 modifications in Arabidopsis tRNAs most likely occur co-transcriptionally before they are exported to the cytoplasm. Due to the deficiency of m¹G and m¹I methylation at position 37, we speculate that hypomethylated tRNAs are unable to efficiently decode their cognate codons or induce frameshifts when entering the ribosome (1,53,54), leading to reduced protein output, particularly those involved in photosynthesis.

The reduced growth rate and defects in reproductive growth illustrate the importance of m¹G37 in plant, consistent with studies about the function of m¹G37 in frame maintenance during translation. In the 'Dual-Error' model, the increased +1 frameshift is not directly mediated by a quadruple base-pairing by unmethylated guanosine at posi-

tion 37 (55), but rather by a compromised ribosomal A-site tRNA and a reduced competence of ribosomal P-site tRNA after translocation (1). We found that in *atrm5a* knock-out mutant, where m¹G nucleoside level was reduced to circa 50% and m¹I to only 20% of that in wild type, the pool of tRNAs could not translate messenger RNAs well, and a negative impact on translation was supported by alteration on the ribosomal profiles (56). Due to technical limitations of current proteomics analysis, the differentially expressed proteins (DEPs) might not reveal a complete picture of differences between wild type and the *atrm5a* mutant. However, these data do support a link between tRNA m¹G/m¹I deficiency with gene/protein expression and phenotypes. In fast growing cells, especially in shoot apex during early growth stage, rapid cell division and expansion demand efficient transcription and translation. It is plausible to explain a 'catch-up' effect during later growth stages where the requirements of tRNAs and the translation machinery are less demanding. Still the specific phenotype on stamen filament elongation is intriguing.

Almost all critical residues are conserved around the catalytic center within the D3/MTase domain. The amino acid conservation allowed us to super-impose AtTrm5a protein on already existing structures in *M. jannaschii* or *Pyrococcus abyssi* (57,58). We tried to crystallize the AtTrm5a protein but failed possibly due to the high flexibility of the D1 domain. Deletion of D1 domain reduces, but does not eliminate, methylation activity *in vitro* (Figure 2F), and did not influence the protein stability or subcellular localization (Supplementary Figure S6). On the contrary, deletion of the D2 domain renders the protein unstable, suggesting D2 domain is necessary for both structural stability and catalysis of m¹G/m¹G methylation. This is also consistent with the structural model, where D2 is in close contact with D3/MTase domain (Figure 1C).

In summary, we have identified *AtTRM5a* gene for m¹G and m¹I modification on position 37 in tRNAs. AtTrm5a is nuclear located and is important for ribosome biogenesis, protein translation and plant development. Our work illustrates the importance of tRNA methylation on protein translation, growth and development in Arabidopsis.

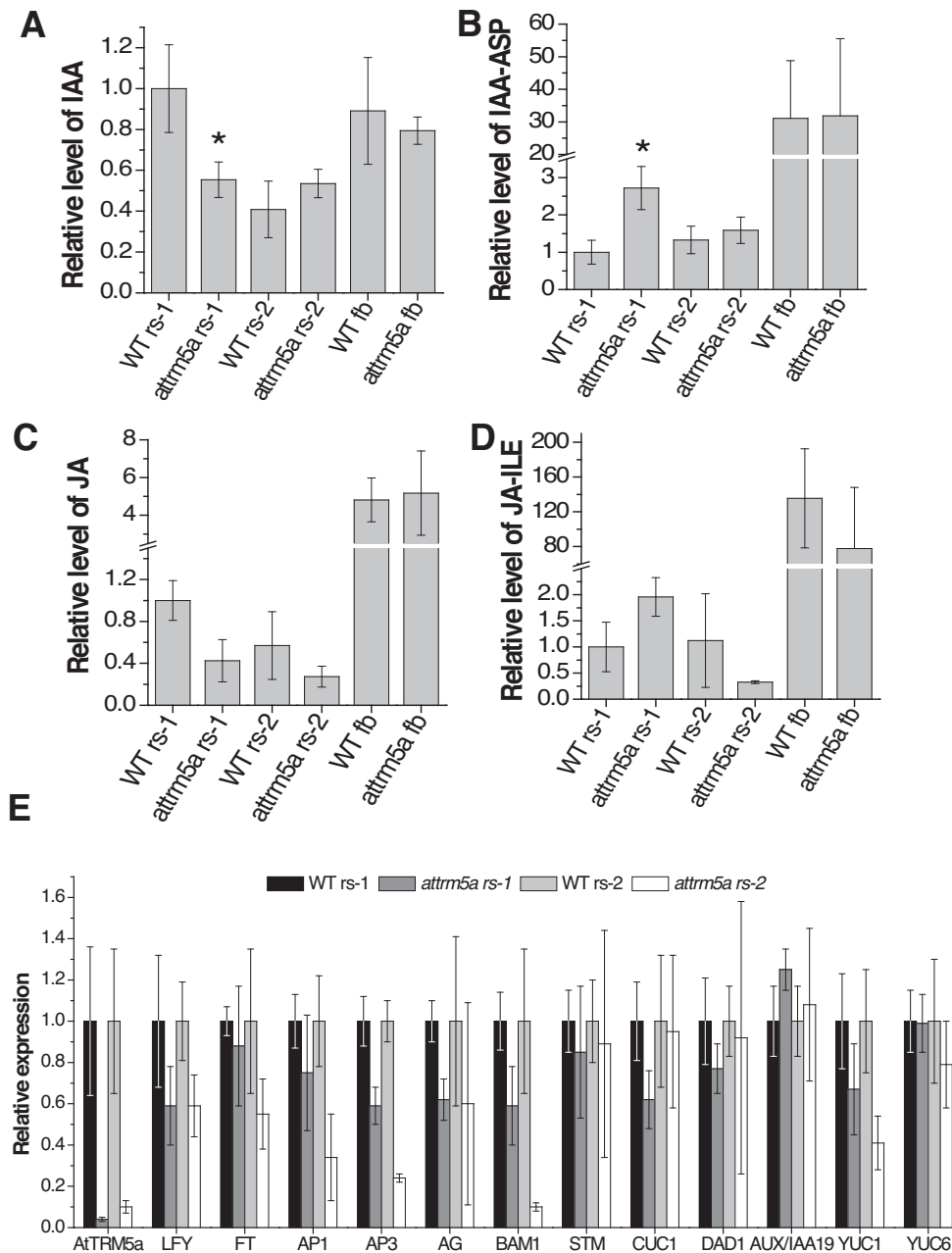


Figure 5. Hormone content measurement and relative expression of flowering and hormone related genes in *atrm5a* mutant and wild type. (A, B) Quantification of indole 3-acetic acid (IAA) and IAA-Asp in wild type and *atrm5a* mutant. Rs-1, rosette leaves of four-week-old plants; rs-2, rosette leaves of 7-week-old plants; fb, flower buds. (C, D) Quantification of jasmonate and JA-ILE in wild type and *atrm5a* mutant. Data from three biological replicates, * or ** indicated significant difference at $P \leq 0.05$ or $P \leq 0.01$, by Student's *t*-test. (E) Relative expression of genes involved in flowering, shoot apex size control, and hormone synthesis/signalling. rs-1, rosette leaves of 4-week-old plants; rs-2, rosette leaves of 7-week-old plants. Gene relative expression in wild-type was set to 1.0. Data from three biological replicates, two technical repeats for each qRT reaction.

DATA AVAILABILITY

ABRC is an open source for Arabidopsis T-DNA line seeds, <https://abrc.osu.edu/>. Euroscarf is a public resource for obtaining *S. cerevisiae* strains, available at <http://www.euroscarf.de/>. NCBI database provides online blast tool, <https://blast.ncbi.nlm.nih.gov/Blast.cgi>; multiple sequence alignment was performed by online ClustalX 2.0 at EMBL-EBI, <https://www.ebi.ac.uk/Tools/msa/clustalw2/>,

and Genedoc software free downloaded from (<http://www.softpedia.com/get/Science-CAD/GeneDoc.shtml>). Protein secondary structure was predicted by Phyre2 (<http://www.sbg.bio.ic.ac.uk/phyre2/html/page.cgi?id=index>). The mass spectrometry proteomics data have been deposited to the ProteomeXChange Consortium via the PRIDE partner repository (<https://www.ebi.ac.uk/pride/archive/>) with the dataset identifier PXD009770.

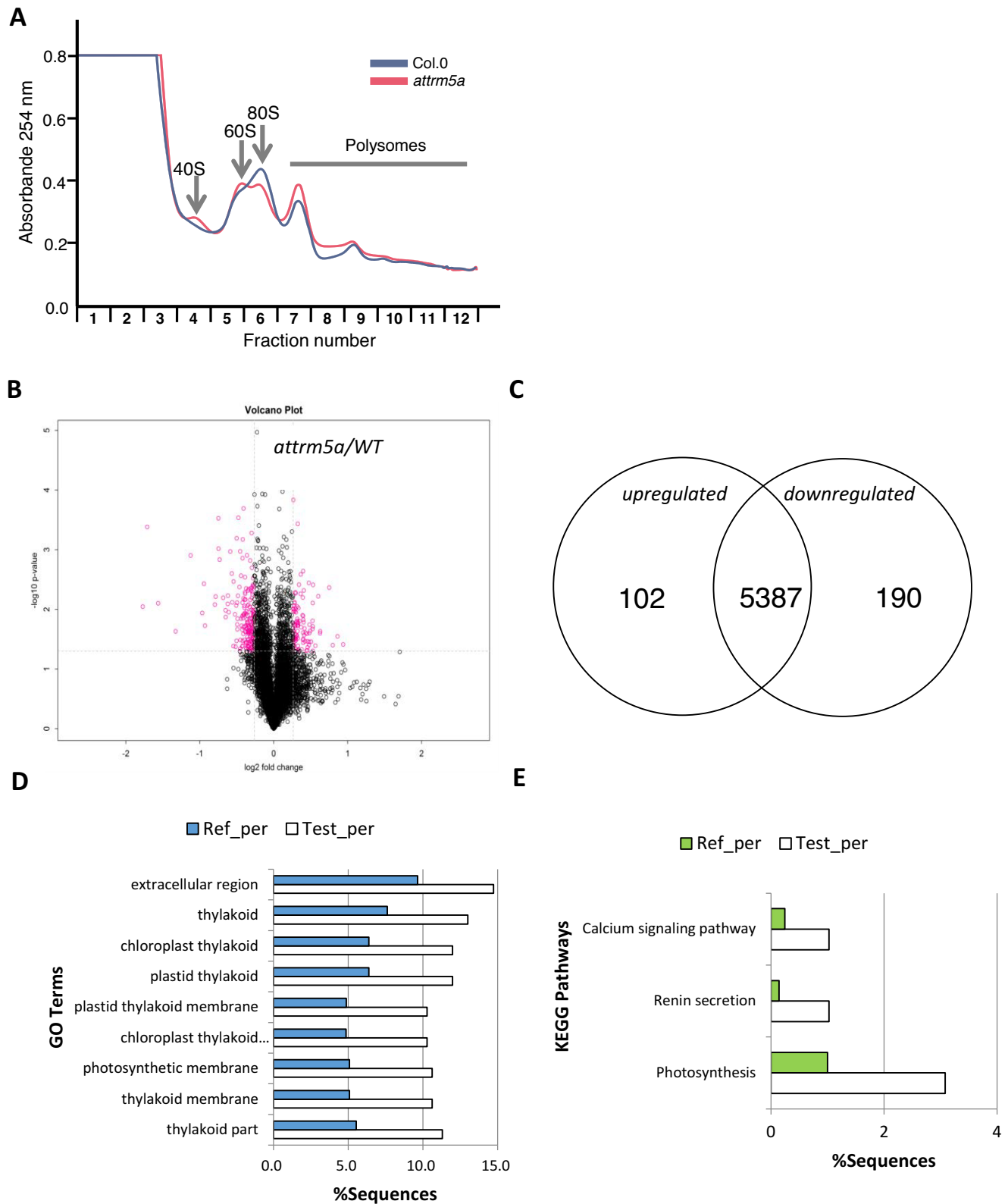


Figure 6. Proteomics analysis and ribosomal profiling between wild type and *attrm5a* mutant. (A) Ribosomal profiling of *attrm5a* mutant. Polysome profiling assays were performed using 3-weeks-old seedlings with 15–45% sucrose density. A254 absorption was monitored. Fractions containing 40s, 60s ribosomal subunits, 80s (monosome) and polysomes were indicated. Wild type profile in blue, *attrm5a* profile in red. (B) Volcano plot of differentially expressed proteins (DEPs) between wild type and *attrm5a* mutant using four-week-old soil-grown plants. (C) Venn Diagram showing up-regulated and down-regulated proteins in *attrm5a* mutant. DEP threshold, fold change ≤ 0.80 or ≥ 1.20 , significance level $P \leq 0.05$. (D, E) GO and KEGG terms enrichment analysis. Each DEP was first annotated in GO or KEGG database, enrichment analysis was performed based on annotated DEPs in wild type and *attrm5a* mutant.

Table 2. Top DEPs (differential expressed proteins) from proteomics analysis

Accession	Description	attrm5a/WT	P value	KO	MapID	Map name
Down-regulated proteins:						
AT5G47380.1	Protein of unknown function, DUF547	0.293	0.009	n.a.		
AT3G26290.1	cytochrome P450, family 71, subfamily B, polypeptide 26	0.305	0.000	K00517	ko00363	Bisphenol degradation
AT1G55040.1	zinc finger (Ran-binding) family protein	0.338	0.008	n.a.		
AT1G68070.1	Zinc finger, C3HC4 type (RING finger) family protein	0.398	0.023	n.a.		
AT2G44300.1	Bifunctional inhibitor/lipid-transfer protein/seed storage 2S albumin superfamily protein	0.459	0.001	n.a.		
AT3G01610.1	cell division cycle 48C	0.511	0.011	K14571	ko03008	Ribosome biogenesis in eukaryotes
AT3G49220.1	Plant invertase/pectin methylesterase inhibitor superfamily	0.520	0.004	n.a.		
AT2G41640.2	Glycosyltransferase family 61 protein	0.525	0.019	n.a.		
AT5G15960.1	stress-responsive protein (KIN1) / stress-induced protein (KIN1)	0.576	0.008	n.a.		
AT2G22500.1	uncoupling protein 5	0.580	0.006	K15104		
AT5G40190.1	RNA ligase/cyclic nucleotide phosphodiesterase family protein	0.595	0.000	n.a.		
AT4G28980.2	CDK-activating kinase 1AT	0.596	0.001	n.a.		
Upregulated proteins:						
AT5G64110.1	Peroxidase superfamily protein	1.407	0.023	K00430	ko00940	Phenylpropanoid biosynthesis
AT5G01400.1	HEAT repeat-containing protein	1.419	0.035	K06100	ko03015	mRNA surveillance pathway
AT2G34480.1	Ribosomal protein L18ae/LX family protein	1.438	0.021	K02882	ko03010	Ribosome
AT2G40410.1	Staphylococcal nuclease homologue	1.440	0.015	n.a.		
AT4G08770.1	Peroxidase superfamily protein	1.442	0.008	K00430	ko00940	Phenylpropanoid biosynthesis
AT1G08770.1	prenylated RAB acceptor 1.E	1.443	0.050	n.a.		
AT1G32090.1	early-responsive to dehydration stress protein (ERD4)	1.443	0.019	n.a.		
AT2G45220.1	Plant invertase/pectin methylesterase inhibitor superfamily	1.446	0.004	K01051	ko00040	Pentose and glucuronate interconversions
AT3G59740.1	Concanavalin A-like lectin protein kinase family protein	1.477	0.040	n.a.		
AT2G38530.1	lipid transfer protein 2	1.517	0.006	n.a.		
AT3G49500.1	RNA-dependent RNA polymerase 6	1.544	0.025	K11699		
AT1G48635.1	peroxin 3	1.547	0.023	K13336	ko04146	Peroxisome
AT4G26660.1	unknown	1.683	0.004	n.a.		
AT2G43680.2	IQ-domain 14	1.739	0.040	n.a.		
ATCG00550.1	photosystem II reaction center protein J	1.818	0.028	n.a.		
AT3G22600.1	Bifunctional inhibitor/lipid-transfer protein/seed storage 2S albumin superfamily protein	1.918	0.039	n.a.		

Samples were taken with three biological replicates. Proteins with fold change ≥ 1.40 or ≤ 0.60 and significance level $P \leq 0.05$ by student t-test were presented. AGI accession and gene annotation were extracted from TAIR database. KEGG orthology and pathway ID were presented for each DEPs from KEGG database (<http://www.genome.jp/kegg/kegg2.html>).

Accession numbers for genes appeared in this study: TRM5 (*S. cerevisiae*); AtTrm5a, At3g56120; AtTrm5b, At4g27340; OsTRM5a, Os02g0606300; OsTRM5b, Os01g0390400; PtTRM5a, POPTR_0018s06240g; Pt-TRM5b, POPTR_0011s12780g; PeTRM5, LOC105114381; ZmTRM5, LOC100274674; BnTRM5, LOC106368106; HsTRM5, TRMT5; MjTRM5b, MJ_RS04720; PaTRM5a, PAB_RS00630; PaTRM5b, PAB_RS03940.

SUPPLEMENTARY DATA

Supplementary Data are available at NAR Online.

ACKNOWLEDGMENTS

The yeast mutant strains GBY15 and GBY16 were kindly provided by Prof. Glenn Bjork and Gunilla Jäger (Umea University, Sweden). We thank Dr Dongqin Li (National Key Laboratory of Crop Genetic Improvement, Huazhong Agricultural University) for the help on LC-MS analysis.

FUNDING

Natural Science Foundation of China [31370604 to B.Z., 31100268 to P.C.]; Natural Science Foundation of Hubei Province [2016CFB438 to P.C.]; Fundamental Research Funds for the Central Universities, China

[2662015PY168 to P.C.]; S.P. was funded by an ARC FT grant [FT160100218] and acknowledges an UoM IRRTF (RNC) grant. Y.Q. was funded by the National Key R&D Program of China (2018YFA0106900); Strategic Priority Research Programs (Category A) of the Chinese Academy of Sciences XDA12010313, and Key Research Program of Frontier Sciences, CAS, (QYZDB-SSW-SMC028). Funding for open access charge: National Natural Science Foundation of China [31370604 to B.Z].

Conflict of interest statement. None declared.

REFERENCES

- Bjork, G.R., Durand, J.M., Hagervall, T.G., Leipuviene, R., Lundgren, H.K., Nilsson, K., Chen, P., Qian, Q. and Urbonavicius, J. (1999) Transfer RNA modification: influence on translational frameshifting and metabolism. *FEBS Lett.*, **452**, 47–51.
- Gustilo, E.M., Vendeix, F.A. and Agris, P.F. (2008) tRNAs' modifications bring order to gene expression. *Curr. Opin. Microbiol.*, **11**, 134–140.
- Bjork, G.R. (1995) *tRNA: Structure, Biosynthesis, and Function*. American Society for Microbiology, Washington, DC, pp. 165–205.
- El Yacoubi, B., Bailly, M. and de Crecy-Lagard, V. (2012) Biosynthesis and function of posttranscriptional modifications of transfer RNAs. *Annu. Rev. Genet.*, **46**, 69–95.
- Gu, C., Begley, T.J. and Dedon, P.C. (2014) tRNA modifications regulate translation during cellular stress. *FEBS Lett.*, **588**, 4287–4296.
- Li, J. and Bjork, G.R. (1995) Structural alterations of the tRNA(m1G37)methyltransferase from *Salmonella typhimurium* affect tRNA substrate specificity. *J. Bacteriol.*, **177**, 6593–6600.
- Bjork, G.R., Wikstrom, P.M. and Bystrom, A.S. (1989) Prevention of translational frameshifting by the modified nucleoside 1-methylguanosine. *Science*, **244**, 986–989.
- Bjork, G.R., Jacobsson, K., Nilsson, K., Johansson, M.J., Bystrom, A.S. and Persson, O.P. (2001) A primordial tRNA modification required for the evolution of life? *EMBO J.*, **20**, 231–239.
- Christian, T., Lahoud, G., Liu, C., Hoffmann, K., Perona, J.J. and Hou, Y.M. (2010) Mechanism of N-methylation by the tRNA m1G37 methyltransferase Trm5. *RNA*, **16**, 2484–2492.
- Goto-Ito, S., Ito, T., Ishii, R., Muto, Y., Bessho, Y. and Yokoyama, S. (2008) Crystal structure of archaeal tRNA(m1G37)methyltransferase aTrm5. *Proteins*, **72**, 1274–1289.
- Christian, T., Evilia, C., Williams, S. and Hou, Y.M. (2004) Distinct origins of tRNA(m1G37) methyltransferase. *J. Mol. Biol.*, **339**, 707–719.
- Motorin, Y. and Helm, M. (2011) RNA nucleotide methylation. *Wiley Interdiscip. Rev.: RNA*, **2**, 611–631.
- Schubert, H.L., Blumenthal, R.M. and Cheng, X. (2003) Many paths to methyltransfer: a chronicle of convergence. *Trends Biochem. Sci.*, **28**, 329–335.
- de Crecy-Lagard, V., Brochier-Armanet, C., Urbonavicius, J., Fernandez, B., Phillips, G., Lyons, B., Noma, A., Alvarez, S., Droogmans, L., Armengaud, J. et al. (2010) Biosynthesis of wyosine derivatives in tRNA: an ancient and highly diverse pathway in Archaea. *Mol. Biol. Evol.*, **27**, 2062–2077.
- Christian, T., Gamper, H. and Hou, Y.-M. (2013) Conservation of structure and mechanism by Trm5 enzymes. *RNA (New York, NY)*, **19**, 1192–1199.
- Abe, T., Ikemura, T., Sugahara, J., Kanai, A., Ohara, Y., Uehara, H., Kinouchi, M., Kanaya, S., Yamada, Y., Muto, A. et al. (2011) tRNADB-CE 2011: tRNA gene database curated manually by experts. *Nucleic Acids Res.*, **39**, D210–D213.
- Juhling, F., Morl, M., Hartmann, R.K., Sprinzl, M., Stadler, P.F. and Putz, J. (2009) tRNADB 2009: compilation of tRNA sequences and tRNA genes. *Nucleic Acids Res.*, **37**, D159–D162.
- Dunin-Horkawicz, S., Czerwoniec, A., Gajda, M.J., Feder, M., Grosjean, H. and Bujnicki, J.M. (2006) MODOMICS: a database of RNA modification pathways. *Nucleic Acids Res.*, **34**, D145–D149.
- Czerwoniec, A., Dunin-Horkawicz, S., Purta, E., Kaminska, K.H., Kasprzak, J.M., Bujnicki, J.M., Grosjean, H. and Rother, K. (2009) MODOMICS: a database of RNA modification pathways. 2008 update. *Nucleic Acids Res.*, **37**, D118–D121.
- Machnicka, M.A., Milanowska, K., Osman Oglou, O., Purta, E., Kurkowska, M., Olchowik, A., Januszewski, W., Kalinowski, S., Dunin-Horkawicz, S., Rother, K.M. et al. (2013) MODOMICS: a database of RNA modification pathways—2013 update. *Nucleic Acids Res.*, **41**, D262–D267.
- Jackman, J.E., Montange, R.K., Malik, H.S. and Phizicky, E.M. (2003) Identification of the yeast gene encoding the tRNA m1G methyltransferase responsible for modification at position 9. *RNA*, **9**, 574–585.
- Brule, H., Elliott, M., Redlak, M., Zehner, Z.E. and Holmes, W.M. (2004) Isolation and characterization of the human tRNA-(N1G37) methyltransferase (TRM5) and comparison to the *Escherichia coli* TrmD protein. *Biochemistry*, **43**, 9243–9255.
- Urbonavicius, J., Stahl, G., Durand, J.M.B., Ben Salem, S.N., Qian, Q., Farabaugh, P.J. and Bjork, G.R. (2003) Transfer RNA modifications that alter +1 frameshifting in general fail to affect -1 frameshifting. *RNA (New York, N Y)*, **9**, 760–768.
- Paris, Z., Horakova, E., Rubio, M.A.T., Sample, P., Fleming, I.M.C., Armocida, S., Lukes, J. and Alfonzo, J.D. (2013) The *T. brucei* TRM5 methyltransferase plays an essential role in mitochondrial protein synthesis and function. *RNA (New York, N Y)*, **19**, 649–658.
- Lee, C., Kramer, G., Graham, D.E. and Appling, D.R. (2007) Yeast mitochondrial initiator tRNA is methylated at guanosine 37 by the Trm5-encoded tRNA (guanine-N1)-methyltransferase. *J. Biol. Chem.*, **282**, 27744–27753.
- Gamper, H.B., Masuda, I., Frenkel-Morgenstern, M. and Hou, Y.M. (2015) The UGG isoacceptor of tRNA^{Pro} is naturally prone to frameshifts. *Int. J. Mol. Sci.*, **16**, 14866–14883.
- Tamura, K., Dudley, J., Nei, M. and Kumar, S. (2007) MEGA4: Molecular Evolutionary Genetics Analysis (MEGA) software version 4.0. *Mol. Biol. Evol.*, **24**, 1596–1599.
- Kelley, L.A., Mezulis, S., Yates, C.M., Wass, M.N. and Sternberg, M.J. (2015) The Phyre2 web portal for protein modeling, prediction and analysis. *Nat. Protoc.*, **10**, 845–858.
- Noma, A., Kirino, Y., Ikeuchi, Y. and Suzuki, T. (2006) Biosynthesis of wybutosine, a hyper-modified nucleoside in eukaryotic phenylalanine tRNA. *EMBO J.*, **25**, 2142–2154.
- Yan, M., Wang, Y., Hu, Y., Feng, Y., Dai, C., Wu, J., Wu, D., Zhang, F. and Zhai, Q. (2013) A high-throughput quantitative approach reveals more small RNA modifications in mouse liver and their correlation with diabetes. *Anal. Chem.*, **85**, 12173–12181.
- Wang, Y., Li, D., Gao, J., Li, X., Zhang, R., Jin, X., Hu, Z., Zheng, B., Persson, S. and Chen, P. (2017) The 2'-O-methyladenosine nucleoside modification gene OsTRM13 positively regulates salt stress tolerance in rice. *J. Exp. Bot.*, **68**, 1479–1491.
- Chan, C.T., Dyavaiah, M., DeMott, M.S., Taghizadeh, K., Dedon, P.C. and Begley, T.J. (2010) A quantitative systems approach reveals dynamic control of tRNA modifications during cellular stress. *PLoS Genet.*, **6**, e1001247.
- Sparkes, I.A., Runions, J., Kearns, A. and Hawes, C. (2006) Rapid, transient expression of fluorescent fusion proteins in tobacco plants and generation of stably transformed plants. *Nat. Protoc.*, **1**, 2019–2025.
- Liu, H., Li, X., Xiao, J. and Wang, S. (2012) A convenient method for simultaneous quantification of multiple phytohormones and metabolites: application in study of rice-bacterium interaction. *Plant Methods*, **8**, 2.
- Livak, K.J. and Schmittgen, T.D. (2001) Analysis of relative gene expression data using real-time quantitative PCR and the 2(-Delta Delta C(T)) Method. *Methods*, **25**, 402–408.
- Missra, A. and von Arnim, A.G. (2014) Analysis of mRNA translation states in Arabidopsis over the diurnal cycle by polysome microarray. *Methods Mol. Biol.*, **1158**, 157–174.
- Luczak, M., Marczak, L. and Stobiecki, M. (2014) Optimization of plasma sample pretreatment for quantitative analysis using iTRAQ labeling and LC-MALDI-TOF/TOF. *PLoS One*, **9**, e101694.
- Conesa, A. and Götz, S. (2008) Blast2GO: A comprehensive suite for functional analysis in plant genomics. *Int. J. Plant Genomics*, **2008**, 1–12.
- Chen, P., Jager, G. and Zheng, B. (2010) Transfer RNA modifications and genes for modifying enzymes in *Arabidopsis thaliana*. *BMC Plant Biol*, **10**, 201.

40. Zhang, C. and Jia, G. (2018) Reversible RNA modification N(1)-methyladenosine (m(1)A) in mRNA and tRNA. *Genomics Proteomics Bioinformatics*, **16**, 155–161.
41. Burgess, A., David, R. and Searle, I.R. (2016) Deciphering the epitranscriptome: A green perspective. *J. Integr. Plant Biol.*, **58**, 822–835.
42. Fisher, A.J. and Beal, P.A. (2018) Structural basis for eukaryotic mRNA modification. *Curr. Opin. Struct. Biol.*, **53**, 59–68.
43. Schwartz, S. (2016) Cracking the epitranscriptome. *RNA*, **22**, 169–174.
44. Roignant, J.Y. and Soller, M. (2017) m(6)A in mRNA: An ancient mechanism for Fine-Tuning gene expression. *Trends Genet.*, **33**, 380–390.
45. Goto-Ito, S., Ito, T., Kuratani, M., Bessho, Y. and Yokoyama, S. (2009) Tertiary structure checkpoint at anticodon loop modification in tRNA functional maturation. *Nat. Struct. Mol. Biol.*, **16**, 1109–1115.
46. Tsurui, H., Kumazawa, Y., Sanokawa, R., Watanabe, Y., Kuroda, T., Wada, A., Watanabe, K. and Shirai, T. (1994) Batchwise purification of specific tRNAs by a solid-phase DNA probe. *Anal. Biochem.*, **221**, 166–172.
47. Fujita, Y., Fujita, M., Shinozaki, K. and Yamaguchi-Shinozaki, K. (2011) ABA-mediated transcriptional regulation in response to osmotic stress in plants. *J. Plant Res.*, **124**, 509–525.
48. Nakashima, K. and Yamaguchi-Shinozaki, K. (2013) ABA signaling in stress-response and seed development. *Plant Cell Rep.*, **32**, 959–970.
49. Xiong, L., Lee, H., Ishitani, M. and Zhu, J.K. (2002) Regulation of osmotic stress-responsive gene expression by the LOS6/ABA1 locus in Arabidopsis. *J. Biol. Chem.*, **277**, 8588–8596.
50. Seo, M., Peeters, A.J., Koiwai, H., Oritani, T., Marion-Poll, A., Zeevaert, J.A., Koornneef, M., Kamiya, Y. and Koshiba, T. (2000) The Arabidopsis aldehyde oxidase 3 (AAO3) gene product catalyzes the final step in abscisic acid biosynthesis in leaves. *PNAS*, **97**, 12908–12913.
51. Santiago, J., Dupeux, F., Round, A., Antoni, R., Park, S.Y., Jamin, M., Cutler, S.R., Rodriguez, P.L. and Marquez, J.A. (2009) The abscisic acid receptor PYR1 in complex with abscisic acid. *Nature*, **462**, 665–668.
52. Acosta, I.F. and Farmer, E.E. (2010) Jasmonates. *The Arabidopsis Book*, **8**, e0129.
53. Farabaugh, P.J. and Bjork, G.R. (1999) How translational accuracy influences reading frame maintenance. *EMBO J.*, **18**, 1427–1434.
54. Gamper, H.B., Masuda, I., Frenkel-Morgenstern, M. and Hou, Y.M. (2015) Maintenance of protein synthesis reading frame by EF-P and m(1)G37-tRNA. *Nat. Commun.*, **6**, 7226.
55. Qian, Q., Li, J.N., Zhao, H., Hagervall, T.G., Farabaugh, P.J. and Bjork, G.R. (1998) A new model for phenotypic suppression of frameshift mutations by mutant tRNAs. *Mol. Cell*, **1**, 471–482.
56. Pospisek, M. and Valasek, L. (2013) Polysome profile analysis—yeast. *Methods Enzymol.*, **530**, 173–181.
57. Wang, C., Jia, Q., Chen, R., Wei, Y., Li, J., Ma, J. and Xie, W. (2016) Crystal structures of the bifunctional tRNA methyltransferase Trm5a. *Sci. Rep.*, **6**, 33553.
58. Wu, J., Jia, Q., Wu, S., Zeng, H., Sun, Y., Wang, C., Ge, R. and Xie, W. (2017) The crystal structure of the Pyrococcus abyssi mono-functional methyltransferase PaTrm5b. *Biochem. Biophys. Res. Commun.*, **493**, 240–245.